

Systemic Mesenchymal Stem Cell Treatment Mitigates Structural and Functional Retinal Ganglion Cell Degeneration in a Mouse Model of Multiple Sclerosis

Oliver W. Gramlich^{1,2}, Alexander J. Brown^{3,4}, Cheyanne R. Godwin^{1,2}, Michael S. Chimenti⁵, Lauren K. Boland⁶, James A. Ankrum⁶, and Randy H. Kardon^{1,2}

¹ Department of Ophthalmology and Visual Sciences, The University of Iowa, Iowa City, IA, USA

² Center for the Prevention and Treatment of Visual Loss, Iowa City VA Health Care System, Iowa City, IA, USA

³ Department of Biomedical Research, National Jewish Health, Denver, CO, USA

⁴ Department of Immunology & Microbiology, University of Colorado Anschutz Medical Campus, Aurora, CO, USA

⁵ Iowa Institute of Human Genetics, Carver College of Medicine, The University of Iowa, Iowa City, IA, USA

⁶ Roy J. Carver Department of Biomedical Engineering College, The University of Iowa, Iowa City, IA, USA

Correspondence: Oliver W. Gramlich, Department of Ophthalmology and Visual Sciences, The University of Iowa, 200 Hawkins Dr, Iowa City, IA 52242, USA. e-mail: oliver-gramlich@uiowa.edu

Received: March 23, 2020

Accepted: May 26, 2020

Published: July 10, 2020

Keywords: optic neuritis; EAE; mesenchymal stem cells; pattern-ERG; retinal ganglion cells

Citation: Gramlich OW, Brown AJ, Godwin CR, Chimenti MS, Boland LK, Ankrum JA, Kardon RH. Systemic mesenchymal stem cell treatment mitigates structural and functional retinal ganglion cell degeneration in a mouse model of multiple sclerosis. *Trans Vis Sci Tech.* 2020;9(8):16. <https://doi.org/10.1167/tvst.9.8.16>

Purpose: The purpose of this study was to determine mesenchymal stem cell (MSC) therapy efficacy on rescuing the visual system in the experimental autoimmune encephalomyelitis (EAE) model of multiple sclerosis (MS) and to provide new mechanistic insights.

Methods: EAE was induced in female C57BL/6 mice by immunization with myelin oligodendrocyte glycoprotein (MOG)_{35–55}, complete Freund's adjuvant, and pertussis toxin. The findings were compared to sham-immunized mice. Half of the EAE mice received intraperitoneally delivered stem cells (EAE + MSC). Clinical progression was monitored according to a five-point EAE scoring scheme. Pattern electroretinogram (PERG) and retinal nerve fiber layer (RNFL) thickness were measured 32 days after induction. Retinas were harvested to determine retinal ganglion cell (RGC) density and prepared for RNA-sequencing.

Results: EAE animals that received MSC treatment seven days after EAE induction showed significantly lower motor-sensory impairment, improvement in the PERG amplitude, and preserved RNFL. Analysis of RNA-sequencing data demonstrated statistically significant differences in gene expression in the retina of MSC-treated EAE mice. Differentially expressed genes were enriched for pathways involved in endoplasmic reticulum stress, endothelial cell differentiation, HIF-1 signaling, and cholesterol transport in the MSC-treated EAE group.

Conclusions: Systemic MSC treatment positively affects RGC function and survival in EAE mice. Better cholesterol handling by increased expression of Abca1, the cholesterol efflux regulatory protein, paired with the resolution of HIF-1 signaling activation might explain the improvements seen in PERG of EAE animals after MSC treatment.

Translational Relevance: Using MSC therapy in a mouse model of MS, we discovered previously unappreciated biochemical pathways associated with RGC neuroprotection, which have the potential to be pharmacologically targeted as a new treatment regimen.

Introduction

Multiple sclerosis (MS) is a chronic neurodegenerative disease, primarily mediated by autoreactive T

cells, which causes visual impairment, fatigue, motor disabilities, pain, and cognitive deficits. Approximately 2.5 million people, primarily young adults, are afflicted with MS. The average age at disease onset is 30 years, and half of the patients require a wheelchair within

25 years of diagnosis.^{1–3} Vision loss due to acute optic neuritis and subsequent retinal ganglion cell (RGC) loss is the major initial feature in approximately 20 to 45% of cases with MS.⁴ There is a very high likelihood that patients diagnosed with MS by other initial symptoms will have at least one episode of MS-related optic neuritis in the future. Many patients with acute optic neuritis completely recover their vision, but approximately 40% suffer from permanent vision loss. Notably, faster recovery of vision is correlated with onset of treatment and the earlier the treatment starts, the better the prognosis is for visual outcome.^{5,6} Patients with MS with no history of optic neuritis show evidence of RGC loss and thinning of the retinal nerve fiber layer (RNFL), determined by optical coherence tomography (OCT) imaging.⁷ Furthermore, impaired contrast sensitivity in patients with MS correlates with severity of central nervous system (CNS) lesion size,^{8,9} demonstrating that the visual pathway is an important indicator of disease activity, even in patients with MS who have no visual symptoms and no history of optic neuritis.

Approaches using mesenchymal stem cells (MSCs) in animal models and clinical studies have shown considerable promise in reducing the severity of autoimmune-mediated disorders by decreasing effector T-cell populations and promoting T-regulatory cells. There are currently 11 ongoing and 13 completed clinical trials worldwide using different sources of MSC (bone marrow-derived, umbilical cord-derived, etc.) and multiple routes of administration for treatments (clinicaltrials.gov). One of the first clinical safety studies using MSCs in patients with secondary progressive MS indicated preservation of RNFL thickness and improvement of visual function after MSC administration.¹⁰ It is known that MSC has immunomodulatory properties that can directly suppress T-cell activation¹¹ and likely serve to reduce CNS damage. Moreover, recent studies have shown that MSC secrete a large variety of trophic factors, such as platelet-derived growth factor, hepatocyte growth factor, and insulin-like growth factor to promote retinal neuroprotection.^{11,12} MSCs are also considered capable of triggering remyelination,¹³ but mechanisms are not well understood. Discovery of biochemical pathways through which MSCs improve visual function and facilitate RGC neuroprotection after an inflammatory demyelinating event could provide new therapeutic targets that can be augmented more specifically through small molecules, drugs, diet, or gene-therapeutic approaches.

The purpose of our study is to overcome this knowledge gap by validating systemic MSC therapy efficiency on rescuing the visual system using the myelin oligo-

dendrocyte glycoprotein (MOG)_{35–55} induced experimental autoimmune encephalomyelitis (EAE) model. We sought to provide data showing that systemic MSC treatment significantly reduces motor-sensory impairment in EAE mice. Furthermore, we used pattern electroretinography (PERG) recordings to indicate rescue of the PERG amplitude in MSC-treated mice, and measurement of RNFL to indicate preservation of axons. Bioinformatics of the retina, including optic nerve tissue, was used to characterize gene expression to discover processes related to RGC death (e.g. HIF-1 pathway activation and endoplasmic reticulum [ER] unfolded protein response), in MSC-treated EAE mice when compared to untreated EAE mice. Moreover, we identified differentially regulated gene clusters associated with endothelial cell differentiation, visual system development, and response to retinoic acid that also influence regulation of cholesterol transport in EAE mice having received systemic MSC treatment. These data indicate that MSC treatment in EAE-mediated optic neuritis involves previously unappreciated pathways associated with neuroprotection and repair of visual system impairments that may be future targets for therapeutics.

Methods

Animals and EAE Induction

All animal experiments were approved by the Iowa City VA Health Care System Institutional Animal Care and Use Committee (IACUC) and were conducted in accordance with the ARVO Statement for the Use of Animals in Ophthalmic and Vision Research. Female two month old C57BL/6/J (B6) mice were purchased from Jackson Laboratories (Bar Harbor, ME) and housed on a 12-hour light-dark cycle with food ad libitum. EAE was induced in 40 mice, as described by Bittner et al.¹⁴ by immunization with 200 μ l solution containing 200 μ g MOG_{35–55} (Sigma Aldrich, St. Louis, MO) emulsified with complete Freund's adjuvant (Sigma) containing 2 mg/mL mycobacterium tuberculosis (BD Difco, Franklin Lakes, NJ) subcutaneously at two sites along the back. A group of 20 control mice received a sham immunization with an equal volume of phosphate-buffered saline (PBS) instead of MOG mixed with complete Freund's adjuvant (control [CTRL]). MOG and CTRL mice were injected with 400 ng pertussis toxin in 200 μ l PBS intraperitoneally at day 0 (day of immunization) and again on day two. Clinical progression was monitored daily according to a five-point EAE scoring system by the following criteria: 0 = no symptoms, 0.5 = partial

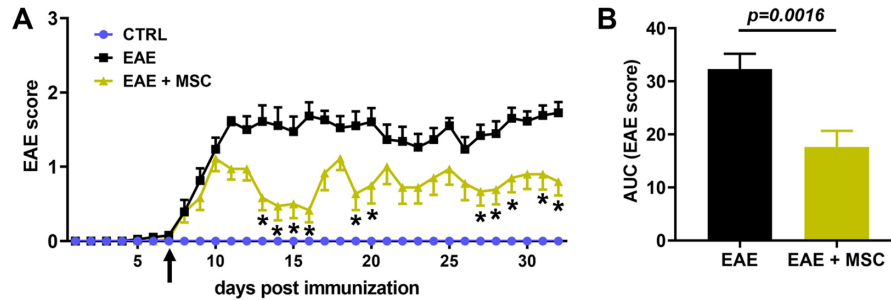


Figure 1. Systemic MSC administration reduces clinical EAE scoring. **(A)** Untreated MOG₃₅₋₅₅-induced EAE mice (*black*: EAE) display a moderate EAE disease course by means of a five-scale EAE scoring system whereas sham-immunized control mice (*blue*: CTRL) show no signs of motor-sensory impairment over time. EAE mice having received as single systemic injection of 10^6 human MSC (*green*: EAE + MSC) at day seven after EAE induction (*arrow*) demonstrate a milder disease course when compared to untreated EAE mice. Mean EAE scores per day with SEM are given and * indicates $P < 0.05$. **(B)** Area under curve (AUC) analysis obtained from MSC-treated and untreated EAE mice demonstrate significantly lower overall disease severity (mean \pm SEM) in MSC-treated EAE mice. Weakening of the tail or any other signs of motor-sensory impairment were not observed in sham-immunized controls.

tail paralysis, 1 = tail paralysis, 1.5 = partial tail paralysis and waddling gait, 2 = tail paralysis and waddling gait, 2.5 = partial limb paralysis, 3 = paralysis of one limb, 3.5 = paralysis of one limb and partial paralysis of another, 4 = paralysis of two limbs, 4.5 = moribund state, and 5 = death (Fig. 1).

MSC Treatment

Human bone marrow derived MSC were obtained from RoosterBio (Frederick, MD). Donor MSC-001 Lot: 00082 was used for all experiments. The MSC were fully characterized and found to meet the ISCT MSC minimal criteria by RoosterBio. MSC were expanded in-house by plating at a density of 5300 MSC/cm² in T-75 flasks and incubated at 37°C. Media was changed every 3 days and passaged using accutase when cells reached 75% confluence. MSC were cultured in minimum essential medium (MEM)- α (Fisher Scientific, Bartlesville, OK) supplemented with 15% premium grade International Serum Industry Association (ISIA) traceable fetal bovine serum (VWR, Radnor, PA), 1% L-glutamine, and 1% penicillin-streptomycin (both Life Technologies, Carlsbad, CA). Twenty EAE mice were randomly selected and received a single injection of 10^6 MSC suspended in 200 μ l PBS via tail vein route at day 7 after EAE induction.

Pattern Electretinography and OCT

Mice were anesthetized with an intraperitoneal injection of ketamine (87.5 mg/kg) and xylazine (2.5 mg/kg) and received 1% tropicamide (Akorn Inc., Lake Forest, IL) for pupil dilation. Animals were kept on heating pads to maintain constant body temperature

between 37 and 38°C for PERG readings. A drop of Genteal gel (Alcon Laboratories, Fort Worth, TX) was placed on the corneal surface. Transient PERG responses were recorded using alternating, reversing, black and white vertical stimuli delivered on a JORVEC (Intelligent Hearing Systems, Miami, FL) system, as previously described by Porciatti's group.¹⁵ Briefly, pattern stimuli of 1 Hz were presented and 372 averaged signals with cut off filter frequencies of 1 to 300 Hz were recorded under mesopic conditions without dark adaptation. P1 latency was determined as the time (millisecond [ms]) from stimulus presentation to the P1 peak and amplitudes (μ V) were calculated from the P1 peak to the N2 trough (Fig. 2A).

After PERG recordings, animals were transferred to a Bioptigen Envisu OCT device (Bioptigen, Morrisville, NC) and volume scans ($1.4 \times 1.4 \times 1.57$ mm) centered at the optic nerve head were obtained. The RNFL was identified as previously described by Antony et al.¹⁶ and RNFL thickness was measured manually at a distance of 400 μ m away from the center of the optic nerve head in the superior, inferior, nasal, and temporal quadrants, and average RNFL thickness was calculated (Fig. 3A). All eyes were inspected for corneal injuries, cataract formation, or insufficient pupil dilation. Subsequently, waveforms or OCT scans of those animals were excluded from further analysis.

RGC Density

Brn3a is accepted as a good marker for RGC¹⁷ and was used for RGC analysis in MSC-treated and untreated EAE mice and controls thirty two days after induction. Eyes of 14 mice per group were

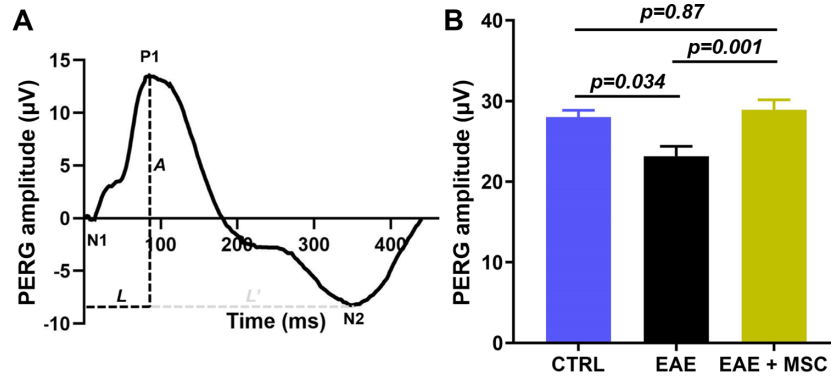


Figure 2. MSC treatment in EAE mice preserves Pattern-ERG amplitude. **(A)** The latency (*L*) was measured as the time from presentation of the stimulus to the P1 peak and the PERG amplitude (*A*) was determined as the distance from the P1 peak to the N2 trough. **(B)** Thirty-two days after induction, sham-immunized controls and MSC-treated EAE mice show almost identical PERG amplitudes, whereas untreated EAE mice demonstrate a significantly declined amplitude. This result indicates a robust MSC-related rescue effect on RGC function.

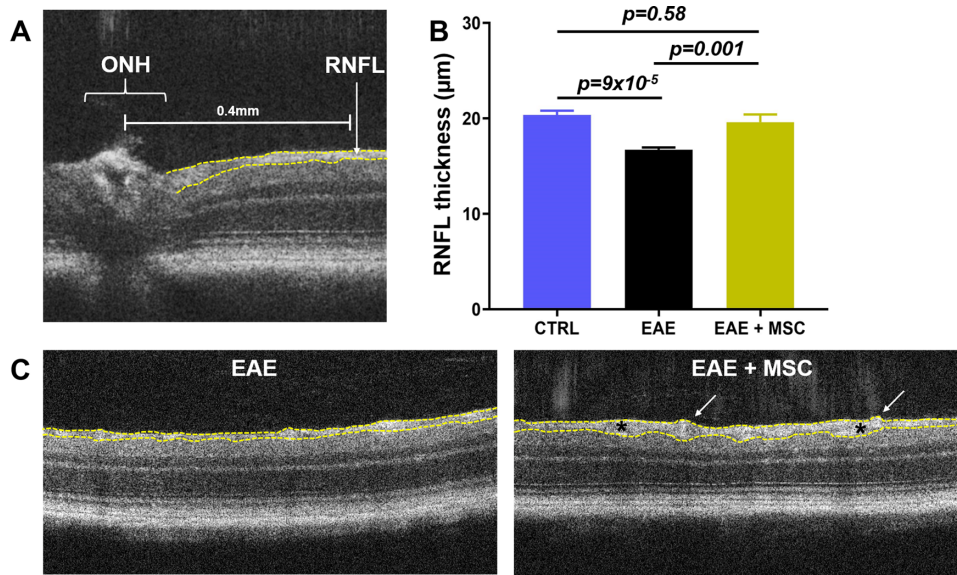


Figure 3. MSC treatment mitigates RNFL thinning in EAE mice. **(A)** Thickness of the RNFL (*dotted yellow lines*) was determined in 4 quadrants at 400 µm distance from the center of the optic nerve head (ONH). **(B)** Treatment of EAE mice with MSC at day 7 leads to preservation of the RNFL thickness when compared to untreated EAE mice, measured 32 days after EAE induction. **(C)** Representative OCT images from EAE mice and MSC-treated EAE mice show differences in RNFL thickness. Note overall thicker RNFL, with areas of RNFL hypertrophy (*between asterisks*) and enlarged blood vessels (*arrows*) in MSC-treated EAE mice.

harvested, fixed in 4% paraformaldehyde for 2 hours, and prepared for wholemount staining. Retinas were permeabilized in 0.3% Triton X-100/PBS for 6 hours followed by a freeze and thaw cycle at -80°C . One percent bovine serum albumin (BSA)/0.3% Triton X-100/PBS was used for 1 hour blocking at room temperature. Retinas were incubated with goat-anti Brn3a primary antibody (Santa Cruz, TX; diluted 1:200 in 1%BSA/0.3% Triton X-100/1% DMSO/PBS) at 4°C for 48 hours on a rocker platform. After washes in PBS, a donkey anti-goat Alexa Fluor 546 secondary antibody solution (Invitrogen, Carlsbad, CA; 1:200 in

PBS) was applied for 3 hours at room temperature in the dark. Following PBS washes, retinas were mounted with Vectashield (Vector Laboratories, Burlingame, CA). Twelve images from each retina were taken at predetermined locations peripherally (5/6), mid-peripherally (3/6), and centrally (1/6) at 20x magnification using an Olympus BX41 microscope (Olympus, Center Valley, PA). Brn3a⁺ cells were counted manually by an observer masked to the protocol using the cell counter plug in ImageJ software (National Institutes of Health, Bethesda, MD). RGC numbers were normalized to density per mm^2 .

Statistics

EAE scores were analyzed using 2-way ANOVA and Bonferroni post hoc test. Furthermore, area under curve (AUC) of the overall disease severity was calculated for every EAE animal and differences between MSC-treated and untreated EAE mice were determined using Mann-Whitney *U* test.¹⁸ PERG amplitude data, RNFL thickness data, and average RGC density were analyzed using 1-way ANOVA followed by Tukey post hoc test. RGC data separated into peripheral, mid-peripheral, and central areas, were analyzed using 2-way ANOVA and subsequent Tukey test. All data are given as mean \pm standard error of the mean (SEM). Calculations were performed using GraphPad Prism version 7.04 (GraphPad Software, San Diego, CA) and *P* values < 0.05 were considered statistically significant.

RNA-Sequencing

To determine relevant processes of RGC neuroprotection preservation of visual function in MSC-treated EAE mice, retinas with posterior optic nerve tissue attached (1 mm) of 6 animals per group were harvested at day 14. RNA was extracted using RNeasy Mini Kit (Qiagen, Germantown, MD) according to the manufacturers' protocol. Six replicates were prepared in each condition (CTRL, EAE, and EAE + MSC). Barcoded samples were pooled and sequenced using an Illumina HiSeq 4000 in the Iowa Institute of Human Genetics (IIHG) Genomics Core Facility.

Bioinformatic Analysis

Reads were demultiplexed and FASTQ data were processed with “bcbio,” a best-practices pipeline available at the open-source “bcbio-nextgen” project (<https://github.com/chapmanb/bcbio-nextgen>; version 1.0.8). Alignment was carried out against the ensemble reference “mm 10” (genome FASTA and annotations derived from ftp://ftp.ensembl.org/pub/release-97/fasta/mus_musculus/) reference genome using the ultra-rapid “hisat2” aligner.¹⁹ Mean number of aligned reads per sample was 66 M, yielding a 79.5% average alignment rate. Concurrently, reads were also “pseudo-aligned” to the mm 10 transcriptome using the “salmon” aligner.²⁰ Transcript-level abundances were converted to gene-level counts using the “tximport” package²¹ from Bioconductor (<https://www.bioconductor.org/>). Quality control (QC) was performed with “qualimap,”²² “fastqc” (<https://www.bioinformatics.babraham.ac.uk/projects/fastqc/>) and “samtools,”²³ computational tools that detect common QC problems. All samples passed

standard QC checks for sequencing and mapping quality. Gene-level counts were used for differential gene expression analysis with “DESeq2.”²⁴ One sample (of six replicates) was dropped from the control group for being an extreme outlier. Differentially expressed (DE) gene lists were analyzed using Advaita Bio’s “iPathwayGuide” (<https://www.advaitabio.com/ipathwayguide>) using the Kyoto Encyclopedia of Genes and Genomes (KEGG) database (version 90.0)²⁵ and gene ontologies from the Gene Ontology Consortium database (version 2019 April 26).²⁶

Results

Systemic MSC Treatment Significantly Lessens Motor-Sensory Impairment in EAE Mice

Following EAE induction using MOG_{35–55} immunization, EAE mice show a monophasic disease course with the first clinical signs present between days 6 and 10 and a peak motor-sensory impairment between days 13 and 16 (Fig 1A). With the first symptoms evident in some EAE animals at days 6 and 7, we decided to start MSC therapy at day 7. MSC have immunomodulatory and neuroprotective features^{27,28} suggesting that administration of MSC in an EAE model would mitigate motor-sensory impairment and rescue EAE-mediated optic neuritis. EAE animals that received MSC treatment still demonstrated motor sensory impairment with a peak at around day 10, but with a significantly less severe clinical manifestation over time (AUC EAE: 32.2 ± 2.9 vs. EAE + MSC: 17.6 ± 2.0 , *P* = 0.0016; Fig 1B).

MSC Treatment of EAE Mice Facilitates Preservation of the PERG Amplitude, Mitigates RNFL Thinning, and Notably Alleviates RGC Loss

Electric activity of RGC significantly contributes to the PERG signal and a decline in the PERG amplitude usually indicates RGC dysfunction or RGC death.^{15,29} We further wanted to investigate if PERG could serve as an outcome measurement to determine disease status and treatment success in EAE mice. Thirty-two days after EAE induction, no differences of the P1 latency were observed among groups (CTRL: 95 ± 5.9 ms, EAE: 84 ± 8.8 ms, and EAE + MSC: 91 ± 3.4 ms, *P* > 0.54). However, we found a significant decline in

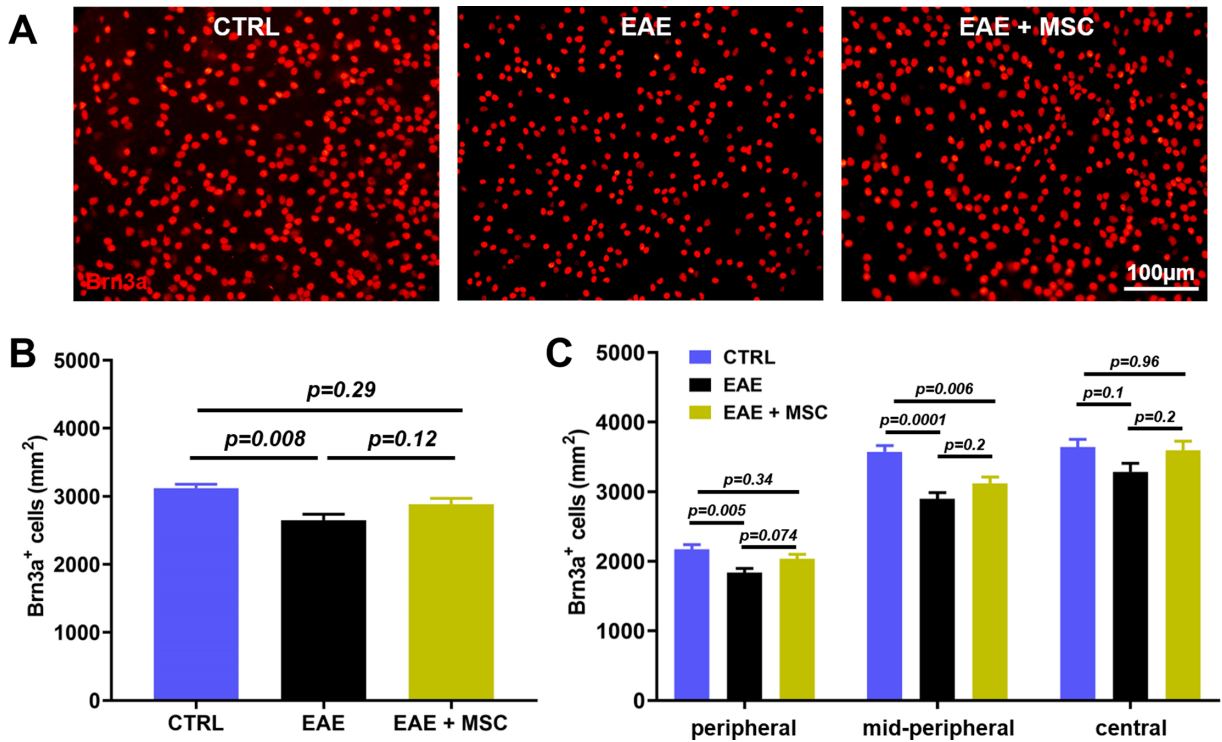


Figure 4. MSC treatment alleviates RGC loss in EAE mice. (A) Representative images of Brn3a immunolabeling (red) display differences in RGC density in the peripheral retina of controls, EAE mice, and MSC-treated EAE mice. (B) Analysis of the average RGC density reveals a significant loss of Brn3a⁺ cells in untreated EAE mice and a remarkably higher RGC density in MSC-treated mice. (C) Regional differences in the RGC density between controls and EAE mice is most prominent in the mid-periphery. A notably upward trend in RGC numbers of EAE mice with MSC treatment is observed in the peripheral and central region, although this is not statistically significant.

the PERG amplitude of EAE animals when compared to sham-immunized controls (CTRL: $28 \pm 0.8 \mu\text{V}$ vs. EAE: $23.2 \pm 1.2 \mu\text{V}$, $P = 0.034$). Furthermore, systemic delivery of human MSCs led to preservation of the PERG amplitude when compared to untreated EAE mice (EAE: $23.2 \pm 1.2 \mu\text{V}$ vs. EAE + MSC: $28.9 \pm 1.2 \mu\text{V}$, $P = 0.001$), whereas no differences in the PERG amplitude were found between MSC-treated EAE mice and CTRLs ($P = 0.87$; Fig. 2B). In our hands, MSC therapy in EAE mice facilitated rescue of RGC function.

Another parameter used to examine progression of MS, and to determine treatment success in a clinical environment, is the measurement of RNFL using OCT. Similar to patients with MS, our EAE mice displayed a significant decline in the average RNFL thickness when compared to controls (CTRL: $20.3 \pm 0.5 \mu\text{m}$ vs. EAE: $16.7 \pm 0.2 \mu\text{m}$, $P = 9 \times 10^{-5}$). This RNFL thinning was mitigated in EAE mice by MSC therapy when compared to untreated EAE mice (EAE: $16.7 \pm 0.2 \mu\text{m}$ vs. EAE + MSC: $19.6 \pm 0.8 \mu\text{m}$, $P = 0.001$; Fig. 3B). Besides normal RNFL thickness, MSC-treated EAE mice displayed sporadic RNFL hypertrophy in areas with enlarged blood vessel formation (Fig. 3C); those

areas have been excluded from RNFL thickness analysis.

Because it is widely accepted that thinning of the RNFL in EAE is usually a result of RGC degeneration, we wanted to determine whether systemic administration of MSC ameliorates RGC loss in EAE mice. Brn3a immunostaining of retinal wholemounts results in a robust labelling of RGC (Fig. 4A) and RGC density was quantified as Brn3a⁺ cells per mm². Four images were taken of each region of the retina peripherally, mid-peripherally, and centrally. RGC numbers follow a gaussian distribution and no statistical differences in any of the areas within groups were found (data not shown). Analysis of the average Brn3a⁺ cell number between controls and EAE mice indicates a significant RGC loss in EAE mice (CTRL: 3121 ± 58 vs. EAE: 2650 ± 89 Brn3a⁺ cells per mm², $P = 0.008$). EAE mice having received MSC treatment show a less dramatic RGC loss and RGC numbers are notably higher when compared to untreated EAE mice (EAE: 2650 ± 89 vs. EAE + MSC: 2886 ± 85 Brn3a⁺ cells per mm², $P = 0.12$; Fig. 4B).

Subsequent analysis of regional differences in RGC loss further indicates that RGC loss in EAE mice

is significant in both peripheral and mid-peripheral regions in comparison to sham-immunized controls. RGC data on EAE mice having received MSC treatment specifies a notable upward trend in Brn3a⁺ RGC numbers between MSC-treated and untreated EAE mice, most prominent in the periphery (EAE: 1837 ± 62 vs. EAE + MSC: 2037 ± 63 Brn3a⁺ cells per mm², $P = 0.07$; Fig. 4C). In accordance with improvement of the PERG amplitude and preservation of the RNFL thickness, MSC treatment in EAE mice also facilitates a notable and almost statistically significant rescue of RGC in the peripheral retina.

MSC Therapy Reduces Endoplasmic Reticulum Stress and HIF-1 Signaling, and Positively Affects Cholesterol Metabolism in Retinas and Optic Nerves of EAE Mice

To get a new mechanistic insight on how systemic administration of MSC into EAE mice facilitates neuroprotection of RGC in EAE mice, we conducted RNA-sequencing of ocular tissue, including the retina and posterior parts of the optic nerve. Because the MSC are of human origin and we were particularly interested in the mouse's retinal response, we filtered for mouse gene signatures. Given > 90% of MSC are known to be cleared by 3 days post-systemic infusion,^{30,31} we did not expect to detect dramatic changes in the retina, but rather a moderate retinal response. Therefore, we chose a more liberal setting with a false discovery rate-adjusted P value of 0.1 for statistical significance and a log fold change of expression with absolute value of at least 0.5. Using these criteria for the comparison of MSC-treated EAE mice to untreated EAE animals, we found 259 differentially expressed genes out of a total of 15,492 genes with measured expression (Fig. 5A).

Major differences in downregulated expression were detected for genes related to the HIF-1 signaling pathway ($P = 0.02$), and processes related to visual system development ($P = 2.8 \times 10^{-4}$) and ER unfolded protein response ($P = 2.3 \times 10^{-4}$). The significant downregulation of hypoxia-inducible factor prolyl hydroxylase 2 gene (Egln1: logFC = -0.54, $P = 8 \times 10^{-4}$) and Heme Oxygenase 1 gene (Hmox1: logFC = -0.57, $P = 0.025$; Fig. 5B), indicated reduced HIF-1 pathway activation in EAE mice with MSC treatment.

Several genes of the crystallin β - γ superfamily were found to be significantly downregulated (Cryba1: logFC = -4.4, $P = 0.027$; Crybb2: logFC = -4.4, $P = 0.045$; Crygc: logFC = -5.9, $P = 0.025$; Fig. 5D). Their functions play crucial roles in lens development,

and, more importantly, in the context of EAE, in RGC protection, astrogliosis, and vascular remodeling, and in unfolded protein responses.³²⁻³⁴ Congruent to decreased gene expression of β - γ crystallins, we found a downregulation of key genes associated with ER unfolded protein responses (Atf3: logFC = -0.95, $P = 0.045$; Stc2: logFC = -0.85, $P = 0.007$; Ero1l: logFC = -0.53, $P = 0.003$; Fig. 5C).

Notably, some significantly increased expression of single genes in MSC-treated EAE mice could not be annotated to specific biological function clusters. These unique genes encode the Kruppel-like factor 17 (Klf17: logFC = 6.1, $P = 4.7 \times 10^{-4}$), the probable inactive 1-aminocyclopropane-1-carboxylate synthase-like protein 2 (Accsl: logFC = 1.9, $P = 0.005$), the PICALM Interacting Mitotic Regulator (Pimreg: logFC:1.6, $P = 0.018$), and the Transmembrane protein 255B (Tmem255b: logFC = 1.8, $P = 0.026$; see Fig. 5A)

Significantly different regulated processes in MSC-treated EAE mice featured mainly upregulated expression for genes that are associated with endothelial cell proliferation ($P = 2.3 \times 10^{-4}$) and to the cellular response to retinoic acid ($P = 3 \times 10^{-4}$). Significantly upregulated genes were found to be involved in endothelial cell differentiation and migration (Stat5A: logFC = 0.5, $P = 0.01$; Pdgfb: logFC = 0.68, $P = 0.024$; Fig. 5F). Relevant upregulated genes in the cluster of cellular response to retinoic acid were the protein tyrosine kinase 2 beta (Ptk2b: logFC = 0.65, $P = 0.016$) and the ATP-binding cassette transporter 1 (Abca1: logFC = 0.83, $P = 0.012$), whereas expression of retinoic acid receptor alpha (Rara: logFC = -0.55, $P = 0.032$; Fig. 5E) was found to be downregulated.

Taken together, our RNA sequencing data indicated that systemic MSC treatment in EAE mice significantly and sustainably influenced gene expression in the retina and optic nerve. When compared to untreated EAE mice, MSC treatment downregulated gene expression of harmful pathways like HIF-1 signaling and ER stress response. Vice versa, MSC therapy in EAE mice triggered an increase in expression of genes associated with beneficial functions to neuroprotection and repair, such as response to retinoic acid, which is also linked to cholesterol transport.

Discussion

Our present study proves the positive effect of systemic MSC treatment on mitigating motor sensory impairment and protection of RGC function in MOG₃₅₋₅₅-induced EAE mice. This result validates previously published data on the efficiency of MSC

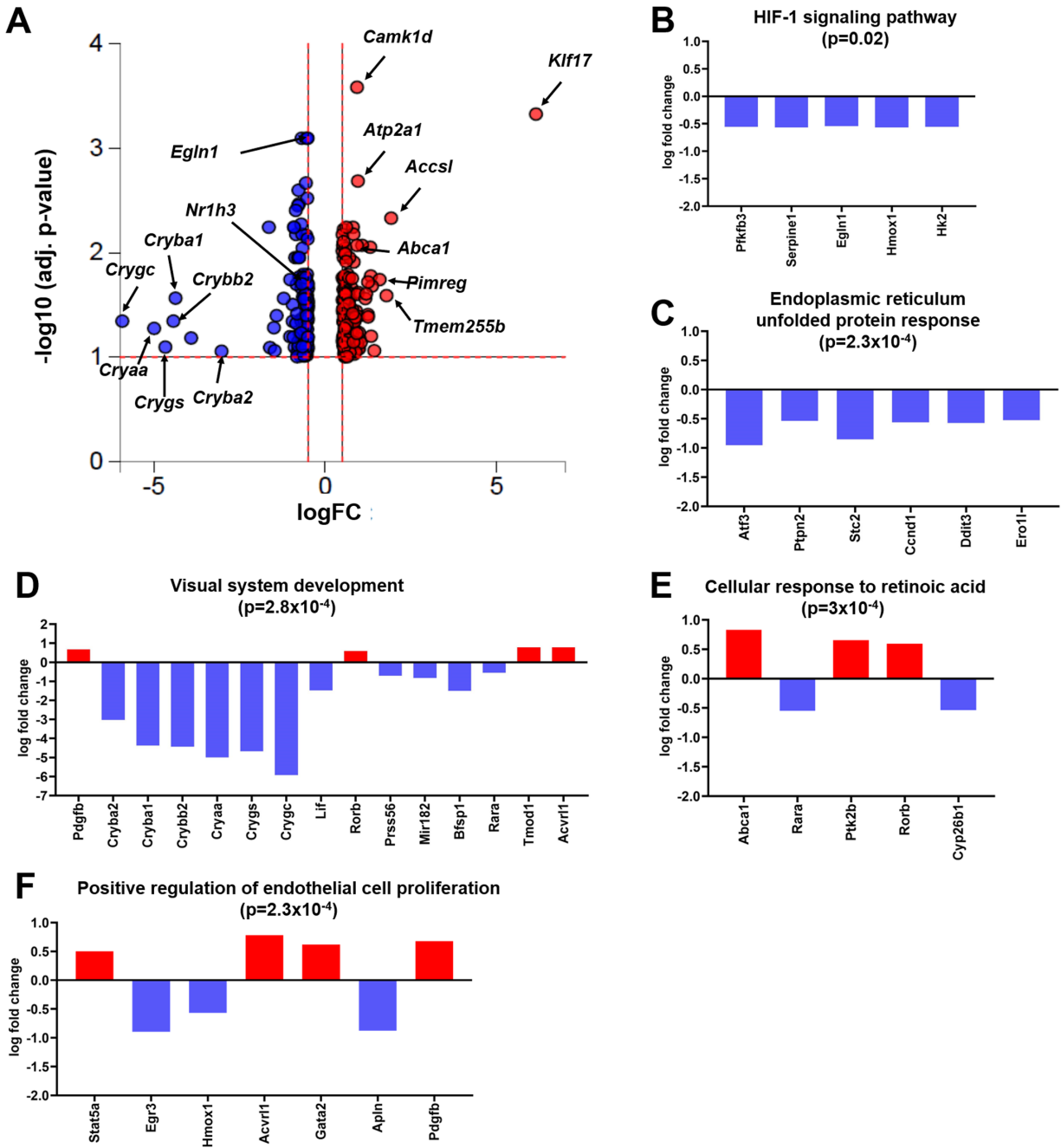


Figure 5. MSC treatment significantly influences gene expression in the retina and optic nerve of EAE mice. **(A)** In the volcano plot, all 259 significantly differentially expressed (DE) genes are represented in terms of their measured expression change (x-axis) and the significance of the change (y-axis). The significance is represented in terms of the negative log (base 10) of the *P* value. The dotted lines represent the thresholds used to select the differentially expressed genes: 0.5 for expression change and 0.1 for significance. The bar plots show the measured gene expression of processes that are found to be significantly differently (*P* value in headlines) regulated in MSC-treated EAE mice. The top five processes are related to **(B)** HIF-1 signaling, **(C)** endoplasmic reticulum unfolded protein response, **(D)** visual system development, **(E)** cellular response to retinoic acid, and **(F)** positive regulation of endothelial cell proliferation. The upregulated genes (positive log fold change) are shown in red, whereas the downregulated genes are blue.

to reduce clinical EAE course in this particular mouse model of MS.³⁵⁻³⁷ Our data provides further evidence that a single systemic administration of 10^6 MSC, an adjusted dosage for mice that is equivalent to what has

been used in clinical studies, is also beneficial on visual function and structure.

Here, we show a preservation of the PERG amplitude as an indicator of RGC viability in MSC-treated

EAE animals and analysis of RNFL thickness reveals a significant rescue effect. Although not strictly identical, these data are comparable to observations made in clinical trials in which patients with secondary progressive MS treated with MSC had preservation of RNFL thickness and an improvement of visual function.¹⁰

We also demonstrate a notable, but nonsignificant, increase in RGC survival upon MSC treatment in our EAE mice by quantification of Brn3a⁺ RGC. Brn3a⁺ is generally a well-accepted RGC marker and is expressed in 80 to 90% of all RGC in the retina.³⁸ However, missing up to 20% of non-Brn3a⁺ RGC could leave additional RGC rescue undetected. Furthermore, it is reported that Brn3a⁺ is transiently downregulated in stressed but surviving RGCs.³⁹ It is conceivable that some surviving RGCs with decreased Brn3a⁺ expression in our MSC-treated EAE group have not been detected, which could have led to an underestimation of the true RGC survival. This outcome might also be due to the nature of the MOG_{35–55} EAE model, in which several studies aimed at RGC neuroprotection have indicated a huge variability in RGC survival from no to almost complete preservation.^{40–42} An important factor on RGC survival in EAE models may be the timing of intervention and response of dosages, as nicely demonstrated by Wilmes et al.⁴¹ The group of Shindler et al. reported a strong correlation on the magnitude RGC survival and the timepoint of corticosteroid intervention in the PLP-induced EAE model.⁴³ We used a single injection of MSC seven days after EAE induction and taking the half-life of MSC into consideration, a single MSC injection rather than multiple administrations might limit longer lasting neuroprotection as indicated by Payne et al.⁴⁴ On the other hand, we see a robust rescue effect of the PERG amplitude, preservation of the RNFL, and notable mitigation of RGC loss, which is indicative of a sustained effect on the visual system. Future experiments should place emphasis on subsequent follow-up MSC injections to increase RGC survival determined by RGC immunolabeling as an outcome measurement in this EAE model.

One major goal of this study was identifying relevant pathways and processes mediating improvement of visual function, RNFL preservation, and RGC neuroprotection due to MSC administration. Our post-treatment RNA-sequencing experiment revealed significant changes in gene expression in the retina and posterior optic nerve of MSC-treated EAE mice when compared to untreated EAE mice. The most striking changes in increased gene expression were found for Tmem255b, Accsl, Pimreg, and Klf-17. The gene Tmem255b, alias FAM70B, encodes the trans-

membrane protein 255b, but the exact function of this protein is yet not clear. One study postulates expression of Tmem255 could serve as a biomarker for assessing the prognosis of patients with muscle-invasive bladder cancer.⁴⁵ Not much is known about the function of the protein coding gene Accsl and Gene Ontology annotations related to this gene include pyridoxal phosphate binding (www.genecards.org). Pimreg, alias FAM64A, is involved in the positive regulation of epi/endothelial-mesenchymal transition (EMT),⁴⁶ whereas Klf-17 is reported to act as a metastasis suppressor in breast cancer and inhibits EMT. The authors could show that downregulation of KLF17 promotes EMT, thus increased expression inhibits EMT. We detected a cluster related to epithelial cell proliferation with downregulation of Erg3 and Apln, genes that promote EMT⁴⁷ and retinal endothelial cell proliferation.⁴⁸ Likewise, we detected upregulated expression of Gata2 that is found to be preventive for epi/endothelial-mesenchymal transformation and beneficial for blood vessel integrity.⁴⁹ Conversely, we also detected an increased gene expression for Stat5a⁵⁰ that would suggest promotion of EMT upon MSC treatment in our model. Derada et al. describes a possible detrimental role of EMT in the context of blood brain barrier dysfunction during MS pathogenesis. The authors also conclude that inhibition of epi/endothelial-mesenchymal transformation might restore blood brain/retina barrier integrity.^{51,52} In our hands, increased Klf-17 expression appears to be associated with prevention of epi/endothelial-mesenchymal transformation and promotion of blood retina barrier repair. More work is needed to confirm the exact role of Klf-17 and FAM64A and its connection to epi- and endothelial function in EAE.

Activation of the HIF-1 signaling pathway affects angiogenesis in neural tissue and increased blood brain barrier permeability.^{53–55} and is associated with the pathology of MS.⁵⁶ Studies in the field of glaucoma have shown that HIF-1 and HIF-1 target genes are elevated and associated with RGC degeneration, but also with survival.^{57–59} Johnson et al. show significant elevation of hypoxia in the gray matter of MOG-induced EAE mice, probably induced by inflammation.^{60,61} The authors further emphasize a detrimental role of HIF-1 signaling in EAE and MS that triggers the upregulation of genes involved in the hypoxia response, but also exacerbates the inflammatory response. Another group confirmed these findings and reported that the increased expression of hypoxia-associated and ER stress related molecules in gray matter lesions originates from microglia cells.⁶² We found a decreased gene expression associated with the

HIF-1 pathway, for ER stress related genes, and corresponding chaperons (the aforementioned crystallin β - γ superfamily) in the retina and optic nerve of MSC-treated EAE mice. Thus, we conjecture that systemic MSC treatment in EAE may facilitate neuroprotection throughout, counterbalancing the HIF-1 pathway activation and hindering the subsequent induction of ER stress induced intrinsic apoptosis in the visual system. More studies are needed to explore the action of these pathways in the EAE model of MS upon MSC treatment.

One likely reason for a significant improvement of motor sensory impairments and visual function in MSC-treated animals is an increased cellular response to retinoic acid that results in the increased expression of *Abca1* and *Ptk2b*. Expression of *Abca1* controls cholesterol metabolism and transport in macrophages/microglia, glia cells, and neurons.^{63,64} Studies in a lysolecithin-induced demyelination model have shown that improper clearance of cholesterol-rich myelin debris increases inflammation and limits remyelination.⁶⁵ The authors used an agonist of the LXR, that controls the expression of genes involved in cholesterol efflux, such as *Abca1*, *Abcg1*, and *ApoE*, and could prove functional improvement on cholesterol handling in macrophages. Thus, augmentation to promote cholesterol recycling via *Abca1* may be a valuable regenerative approach to decrease inflammation and improve remyelination in MS. *Ptk2b*, alias *Pyk2*, is involved in calcium-induced regulation of ion channels and interacts with PSD-95.⁶⁶ Along with the focal-adhesion kinase, *Ptk2b* mediates trophic or anti-apoptotic effects of neurotransmitters that are beneficial for synaptic activity, survival, and plasticity.⁶⁷ It is conceivable that in our EAE model, increased expression of *Ptk2b* triggered by MSC therapy, led to improvement of the PERG amplitude via modulation of neuronal activity at the PSD95 terminals in the inner plexiform layer. Furthermore, expression of *Ptk2b* seems to be a critical upstream regulator in *Chi3l3*-induced oligodendrogenesis,⁶⁸ which could have a positive effect on optic nerve myelination.

In summary, this study provides further insights into the pathways that are modulated by MSC therapy to promote neuroprotection and improvement of visual function in a MOG-induced model of MS. Our results are generally in accordance with findings of previous clinical studies. We further hypothesize that prevention of epi/endothelial-mesenchymal transformation, inhibition of HIF-1 signaling, and augmentation of cholesterol metabolism through retinoic acid might be a viable add-on approach to promote rehabilitation in MS.

Acknowledgments

R.H.K. and O.W.G. are supported by a VA merit grant (C2978-R). L.B. was supported through an NIH training grant (#5T32GM007337). Additional support from the Straub Foundation awarded to J.A.A. was used to complete the project.

Disclosure: **O.W. Gramlich**, None; **A.J. Brown**, None; **C.R. Godwin**, None; **M.S. Chimenti**, None; **L.K. Boland**, None; **J.A. Ankrum**, None; **R.H. Kardon**, None

References

1. Dendrou CA, Fugger L, Friese MA. Immunopathology of multiple sclerosis. *Nat Rev Immunol*. 2015;15:545–558.
2. Korn T. Pathophysiology of multiple sclerosis. *J Neurol*. 2008;255(suppl 6):2–6.
3. Compston A, Coles, A. Multiple sclerosis. *Lancet*. 2008;372:1502–1517.
4. Shams PN, Plant GT. Optic neuritis: a review. *Int MS J*. 2009;16:82–89.
5. Beck RW, et al. A randomized, controlled trial of corticosteroids in the treatment of acute optic neuritis. The Optic Neuritis Study Group. *N Engl J Med*. 1992;326:581–588.
6. Arnold AC. Evolving management of optic neuritis and multiple sclerosis. *Am J Ophthalmol*. 2005;139:1101–1108.
7. Petzold A, et al. Retinal layer segmentation in multiple sclerosis: a systematic review and meta-analysis. *Lancet Neurol*. 2017;16:797–812.
8. Soler Garcia A, et al. Relationship between contrast sensitivity test and disease severity in multiple sclerosis patients. *Arch Soc Esp Ophthalmol*. 2014;89:347–351.
9. Balcer LJ, Frohman EM. Evaluating loss of visual function in multiple sclerosis as measured by low-contrast letter acuity. *Neurology*. 2010;74(suppl 3):S16–S23.
10. Connick P, et al. Autologous mesenchymal stem cells for the treatment of secondary progressive multiple sclerosis: an open-label phase 2a proof-of-concept study. *Lancet Neurol*. 2012;11:150–156.
11. Gramlich OW, et al. Cryopreserved mesenchymal stromal cells maintain potency in a retinal ischemia/reperfusion injury model: toward an off-the-shelf therapy. *Sci Rep*. 2016;6:26463.
12. Shi M, Liu ZW, Wang FS. Immunomodulatory properties and therapeutic application of

- mesenchymal stem cells. *Clin Exp Immunol.* 2011;164:1–8.
13. Rivera FJ, Aigner L. Adult mesenchymal stem cell therapy for myelin repair in multiple sclerosis. *Biol Res.* 2012;45:257–268.
 14. Bittner S, et al. Myelin oligodendrocyte glycoprotein (MOG35-55) induced experimental autoimmune encephalomyelitis (EAE) in C57BL/6 mice. *J Vis Exp.* 2014;86:51275.
 15. Chou TH, et al. Robust mouse pattern electroretinograms derived simultaneously from each eye using a common snout electrode. *Invest Ophthalmol Vis Sci.* 2014;55:2469–2475.
 16. Antony BJ, et al. Automated 3D segmentation of intraretinal surfaces in SD-OCT volumes in normal and diabetic mice. *Transl Vis Sci Technol.* 2014;3:8.
 17. Nadal-Nicolas FM, et al. Brn3a as a marker of retinal ganglion cells: qualitative and quantitative time course studies in naive and optic nerve-injured retinas. *Invest Ophthalmol Vis Sci.* 2009;50:3860–3868.
 18. Tietz SM, et al. Refined clinical scoring in comparative EAE studies does not enhance the chance to observe statistically significant differences. *Eur J Immunol.* 2016;46:2481–2483.
 19. Kim D, Langmead B, Salzberg SL. HISAT: a fast spliced aligner with low memory requirements. *Nat Methods.* 2015;12:357–360.
 20. Patro R, et al. Salmon provides fast and bias-aware quantification of transcript expression. *Nat Methods.* 2017;14:417–419.
 21. Sonesson C, Love MI, Robinson MD. Differential analyses for RNA-seq: transcript-level estimates improve gene-level inferences. *F1000Res.* 2015;4:1521.
 22. Garcia-Alcalde F, et al. Qualimap: evaluating next-generation sequencing alignment data. *Bioinformatics.* 2012;28:2678–2679.
 23. Li H, et al. The Sequence Alignment/Map format and SAMtools. *Bioinformatics.* 2009;25:2078–2079.
 24. Love MI, Huber W, Anders S. Moderated estimation of fold change and dispersion for RNA-seq data with DESeq2. *Genome Biol.* 2014;15:550.
 25. Kanehisa M, Goto S. KEGG: Kyoto encyclopedia of genes and genomes. *Nucleic Acids Res.* 2000;28:27–30.
 26. Ashburner M, et al. Gene ontology: tool for the unification of biology. The Gene Ontology Consortium. *Nat Genet.* 2000;25:25–29.
 27. Kassis I, et al. Neuroprotection and immunomodulation with mesenchymal stem cells in chronic experimental autoimmune encephalomyelitis. *Arch Neurol.* 2008;65:753–761.
 28. Kassis I, Vaknin-Dembinsky A, Karussis D. Bone marrow mesenchymal stem cells: agents of immunomodulation and neuroprotection. *Curr Stem Cell Res Ther.* 2011;6:63–68.
 29. Porciatti V, Saleh M, Nagaraju M. The pattern electroretinogram as a tool to monitor progressive retinal ganglion cell dysfunction in the DBA/2J mouse model of glaucoma. *Invest Ophthalmol Vis Sci.* 2007;48:745–751.
 30. Lee RH, et al. Intravenous hMSCs improve myocardial infarction in mice because cells embolized in lung are activated to secrete the anti-inflammatory protein TSG-6. *Cell Stem Cell.* 2009;5:54–63.
 31. Kidd S, et al. Direct evidence of mesenchymal stem cell tropism for tumor and wounding microenvironments using in vivo bioluminescent imaging. *Stem Cells.* 2009;27:2614–2623.
 32. Fischer D, et al. Crystallins of the beta/gamma-superfamily mimic the effects of lens injury and promote axon regeneration. *Mol Cell Neurosci.* 2008;37:471–479.
 33. Slingsby C, Wistow GJ. Functions of crystallins in and out of lens: roles in elongated and post-mitotic cells. *Prog Biophys Mol Biol.* 2014;115:52–67.
 34. Ma Z, et al. Human betaA3/A1-crystallin splicing mutation causes cataracts by activating the unfolded protein response and inducing apoptosis in differentiating lens fiber cells. *Biochim Biophys Acta.* 2016;1862:1214–1227.
 35. Rafei M, et al. Allogeneic mesenchymal stem cells for treatment of experimental autoimmune encephalomyelitis. *Mol Ther.* 2009;17:1799–1803.
 36. Nasri F, et al. Therapeutic efficacy of mesenchymal stem cells and mesenchymal stem cells-derived neural progenitors in experimental autoimmune encephalomyelitis. *Int J Stem Cells.* 2018;11:68–77.
 37. Bai L, et al. Human bone marrow-derived mesenchymal stem cells induce Th2-polarized immune response and promote endogenous repair in animal models of multiple sclerosis. *Glia.* 2009;57:1192–1203.
 38. Mead B, Tomarev S. Evaluating retinal ganglion cell loss and dysfunction. *Exp Eye Res.* 2016;151:96–106.
 39. Lucas-Ruiz F, et al. Neuronal death in the contralateral un-injured retina after unilateral axotomy: role of microglial cells. *Int J Mol Sci.* 2019;20:5733.
 40. McDougald DS, et al. SIRT1 and NRF2 gene transfer mediate distinct neuroprotective effects upon retinal ganglion cell survival and function in experimental optic neuritis. *Invest Ophthalmol Vis Sci.* 2018;59:1212–1220.

41. Wilmes AT, et al. Laquinimod protects the optic nerve and retina in an experimental autoimmune encephalomyelitis model. *J Neuroinflammation*. 2018;15:183.
42. Khan RS, et al. Effects of varying intranasal treatment regimens in ST266-mediated retinal ganglion cell neuroprotection. *J Neuroophthalmol*. 2019;39:191–199.
43. Dutt M, et al. Timing of corticosteroid therapy is critical to prevent retinal ganglion cell loss in experimental optic neuritis. *Invest Ophthalmol Vis Sci*. 2010;51:1439–1445.
44. Payne NL, et al. Distinct immunomodulatory and migratory mechanisms underpin the therapeutic potential of human mesenchymal stem cells in autoimmune demyelination. *Cell Transplant*. 2013;22:1409–1425.
45. Kang HW, et al. FAM70B as a novel prognostic marker for cancer progression and cancer-specific death in muscle-invasive bladder cancer. *Korean J Urol*. 2012;53:598–606.
46. Zhang J, et al. Up-regulation of FAM64A promotes epithelial-to-mesenchymal transition and enhances stemness features in breast cancer cells. *Biochem Biophys Res Commun*. 2019;513:472–478.
47. Liu D, et al. The zinc-finger transcription factor, early growth response 3, mediates VEGF-induced angiogenesis. *Oncogene*. 2008;27:2989–2998.
48. Kasai A, et al. Apelin is a novel angiogenic factor in retinal endothelial cells. *Biochem Biophys Res Commun*. 2004;325:395–400.
49. Kanki Y, et al. Epigenetically coordinated GATA2 binding is necessary for endothelium-specific endomucin expression. *EMBO J*. 2011;30:2582–2595.
50. Benitah SA, et al. STAT5a activation mediates the epithelial to mesenchymal transition induced by oncogenic RhoA. *Mol Biol Cell*. 2003;14:40–53.
51. Derada Troletti C, et al. Molecular alterations of the blood-brain barrier under inflammatory conditions: the role of endothelial to mesenchymal transition. *Biochim Biophys Acta*. 2016;1862:452–460.
52. Derada Troletti C, et al. Inflammation-induced endothelial to mesenchymal transition promotes brain endothelial cell dysfunction and occurs during multiple sclerosis pathophysiology. *Cell Death Dis*. 2019;10:45.
53. Hashimoto T, Shibasaki F, Hypoxia-inducible factor as an angiogenic master switch. *Front Pediatr*. 2015;3:33.
54. Yuen TJ, et al. Oligodendrocyte-encoded HIF function couples postnatal myelination and white matter angiogenesis. *Cell*. 2014;158:383–396.
55. Nakamura-Ishizu A, et al. The formation of an angiogenic astrocyte template is regulated by the neuroretina in a HIF-1-dependent manner. *Dev Biol*. 2012;363:106–114.
56. Lengfeld J, Cutforth T, Agalliu D. The role of angiogenesis in the pathology of multiple sclerosis. *Vasc Cell*. 2014;6:23.
57. Ergorul C, et al. Hypoxia inducible factor-1alpha (HIF-1alpha) and some HIF-1 target genes are elevated in experimental glaucoma. *J Mol Neurosci*. 2010;42:183–191.
58. Tezel G, Wax MB. Hypoxia-inducible factor 1alpha in the glaucomatous retina and optic nerve head. *Arch Ophthalmol*. 2004;122:1348–1356.
59. Zhu Y, Zhang L, Gidday JM. Role of hypoxia-inducible factor-1alpha in preconditioning-induced protection of retinal ganglion cells in glaucoma. *Mol Vis*. 2013;19:2360–2372.
60. Johnson TW, et al. Gray matter hypoxia in the brain of the experimental autoimmune encephalomyelitis model of multiple sclerosis. *PLoS One*. 2016;11:e0167196.
61. Yang R, Dunn JF. Multiple sclerosis disease progression: contributions from a hypoxia-inflammation cycle. *Mult Scler*. 2019;25:1715–1718.
62. McMahon JM, et al. Increased expression of ER stress- and hypoxia-associated molecules in grey matter lesions in multiple sclerosis. *Mult Scler*. 2012;18:1437–1447.
63. Ramirez CM, et al. MicroRNA-758 regulates cholesterol efflux through posttranscriptional repression of ATP-binding cassette transporter A1. *Arterioscler Thromb Vasc Biol*. 2011;31:2707–2714.
64. Hirsch-Reinshagen V, et al. Deficiency of ABCA1 impairs apolipoprotein E metabolism in brain. *J Biol Chem*. 2004;279:41197–41207.
65. Cantuti-Castelvetri L, et al. Defective cholesterol clearance limits remyelination in the aged central nervous system. *Science*. 2018;359:684–688.
66. Bartos JA, et al. Postsynaptic clustering and activation of Pyk2 by PSD-95. *J Neurosci*. 2010;30:449–463.
67. Girault JA, et al. FAK and PYK2/CAKbeta in the nervous system: a link between neuronal activity, plasticity and survival? *Trends Neurosci*. 1999;22:257–263.
68. Starossom SC, et al. Chi3l3 induces oligodendrogenesis in an experimental model of autoimmune neuroinflammation. *Nat Commun*. 2019;10:217.